Chinese Chemical Letters 37 (2026) 111727

Contents lists available at ScienceDirect

Chinese Chemical Letters

journal homepage: www.elsevier.com/locate/cclet

Macrophage membrane-engineered nanovesicles for targeted delivery of emodin in ulcerative colitis *via* chemotactic homing

Youcheng Hu[a,1], Guichan Li[b,1], Chunli Qi[c], Xiaoyan Lin[c], Xingwang Zhang[b,*], Hao Wang[a,*]

[a] Department of Anesthesiology and Clinical Research Institute, The First Affiliated Hospital of Jinan University, Guangzhou 510630, China
[b] Department of Pharmaceutics, School of Pharmacy, Jinan University, Guangzhou 511443, China
[c] Institute of Laboratory Animals, Jinan University, Guangzhou 510632, China

ARTICLE INFO

Article history:
Received 23 June 2025
Revised 13 August 2025
Accepted 15 August 2025
Available online 16 August 2025

Keywords:
Nanovesicles
Macrophage
Emodin
Ulcerative colitis
Targeted therapy
Chemokine

ABSTRACT

Ulcerative colitis (UC) is a chronic inflammatory bowel disease featured by dysregulated immune responses and compromised intestinal barrier function. Current therapies often suffer from limited efficacy and systemic side effects due to non-specific drug distribution. Here, we developed macrophage membrane-camouflaged nanovesicles (*mc*NVs) for targeted delivery of emodin (Emo) to inflamed colon tissues. The biomimetic nanovesicles were fabricated by fusing J774A.1 macrophage membranes with Emo-loaded liposomes, inheriting the parent cells' chemotactic homing capabilities while maintaining excellent drug loading and colloidal stability. Systematic characterization confirmed successful membrane integration, as evidenced by transmission electron microscope (TEM) imaging, particle size, and ζ potential analyses. *In vitro* studies demonstrated favorable sustained release and enhanced cellular uptake of Emo-loaded *mc*NVs (Emo-*mc*NVs) compared to conventional liposomes. In a sodium dextran sulfate (DSS)-induced murine colitis model, Emo-*mc*NVs exhibited superior colon-targeting capability through chemokine gradient recognition (C-C motif chemokine ligand (CCL)2/3/5), resulting in significantly improved therapeutic outcomes *versus* free Emo and 5-aminosalicylic acid controls. Treatment with Emo-*mc*NVs attenuated disease severity (reduced disease activity index (DAI) score), preserved the colon architecture, and decreased pro-inflammatory cytokines (tumor necrosis factor α (TNF-α), interleukin 1β (IL-1β), IL-6). Biodistribution studies using multimodal imaging confirmed specific accumulation in the inflamed colon tissue with minimal systemic exposure. This study presents a novel biohybrid delivery system that leverages the pathophysiology of UC for targeted therapy, offering a promising translational approach for inflammatory bowel diseases.

© 2026 Published by Elsevier B.V. on behalf of Chinese Chemical Society and Institute of Materia Medica, Chinese Academy of Medical Sciences.

Ulcerative colitis (UC), a chronic and relapsing inflammatory bowel disease (IBD), is characterized by diffuse mucosal inflammation in the colon, leading to debilitating symptoms such as abdominal pain, bloody diarrhea, and increased cancer risk [1,2]. Current therapies, including aminosalicylates, corticosteroids, and biologics, often suffer from systemic toxicity, off-target effects, or limited efficacy due to the complex inflammatory microenvironment of UC [3,4]. Thus, there is an urgent need for targeted drug delivery systems that can selectively accumulate in inflamed colon tissues while minimizing adverse effects.

Emodin (Emo), a natural anthraquinone derived from *Rheum Palmatum*, has demonstrated potent anti-inflammatory, antioxidant, and intestinal barrier-repairing properties in UC models [5–7]. However, its clinical translation is hindered by poor solubility, nonspecific biodistribution, and potential systemic toxicity at high doses [8]. To address these challenges, biomimetic nanotechnology leveraging cell membranes has emerged as a promising strategy for targeted drug delivery [9–12]. Specifically, these biomimetic systems exhibit multiple critical delivery advantages, including bio-guided targeting capability, enhanced immune evasion, and stimuli-responsive drug release. Macrophages, as key players in UC pathogenesis, inherently possess chemotactic homing capabilities toward inflamed sites *via* chemokine receptor-ligand interactions (*e.g.*, C–C chemokine receptor type 2-C-C motif chemokine ligand 2 (CCR2-CCL2)) [13–16]. By cloaking nanovesicles with macrophage membranes, these vesicles can inherit the parent cells' tropism for inflammatory loci, enabling precise drug delivery.

Herein, we developed macrophage membrane-camouflaged nanovesicles (*mc*NVs) for the targeted delivery of Emo to UC

* Corresponding authors.
E-mail addresses: zhangxw@jnu.edu.cn (X. Zhang), haowang@jnu.edu.cn (H. Wang).
[1] These authors contributed equally to this work.

https://doi.org/10.1016/j.cclet.2025.111727
1001-8417/© 2026 Published by Elsevier B.V. on behalf of Chinese Chemical Society and Institute of Materia Medica, Chinese Academy of Medical Sciences.

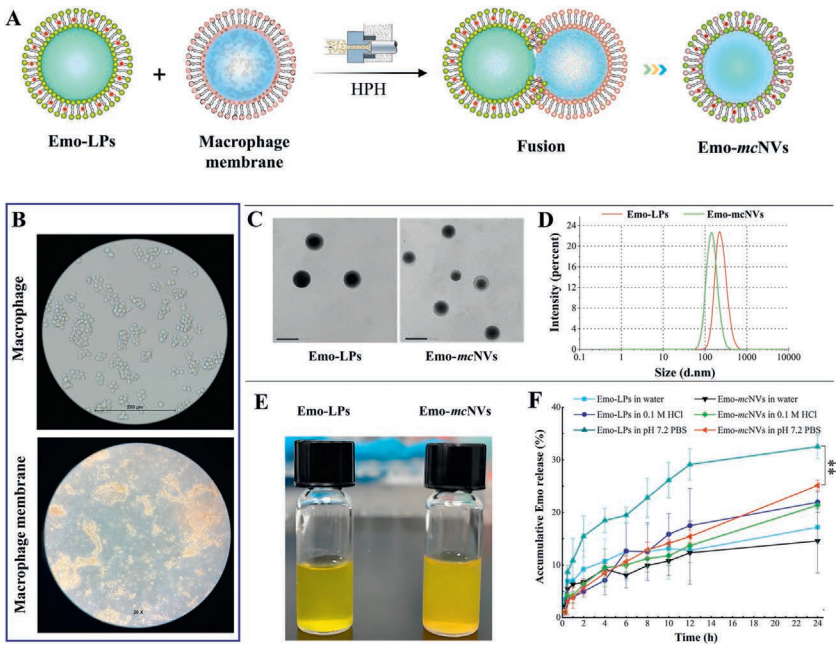


Fig. 1. Fabrication and characterization of Emo-*mc*NVs. (A) Schematic of the fabrication process. HPH, high-pressure homogenization. (B) Microscopic appearance of macrophage and macrophage-derived membrane. (C) TEM images of Emo-LPs and Emo-*mc*NVs. Scale bar: 500 nm. (D) Size distribution of Emo-LPs and Emo-*mc*NVs. (E) Macroscopic appearance of Emo-LPs and Emo-*mc*NVs. (F) *In vitro* Emo release profiles from Emo-LPs and Emo-*mc*NVs over 24 h, paired *t*-test. $M = \text{mol/L}$. $^{**}P < 0.01$. Data expressed as mean ± standard deviation (SD) ($n = 3$).

lesions. The *mc*NVs combine the biological advantages of macrophage membranes [17], such as inflammatory chemotaxis and immune evasion, with the high drug-loading capacity and stability of synthetic liposomes. We hypothesized that *mc*NVs would actively target the inflamed colon *via* macrophage-mimicking chemotaxis, thereby enhancing Emo's therapeutic efficacy while reducing off-target effects. The engineered *mc*NVs are anticipated to specifically accumulate in UC tissues through chemotactic homing, thereby enhancing targeted delivery of the payload to inflammatory loci, potentiating its anti-inflammatory effects and promoting epithelial repair. This biomimetic platform may advance UC therapy while providing a generalizable strategy for targeted delivery in other inflammatory diseases.

Building upon our previous engineering of selenized liposomes for Emo delivery [18], we demonstrated that selenization significantly ameliorated liposomal structural stability, though it did not translate to enhanced oral bioavailability. This dichotomy suggested that structural stabilization alone might be insufficient for oral delivery but could prove valuable for localized therapeutic applications. To transcend this limitation through biomimetic engineering, we developed Emo-loaded *mc*NVs (Emo-*mc*NVs) using a common lipid membrane fusion approach (Fig. 1A) [19]. Successful fabrication of Emo-*mc*NVs was systematically verified through multi-modal characterization. The fabrication process began with J774A.1 macrophage membrane isolation through five freeze-thaw cycles (−80/37 °C) followed by differential centrifugation [20], which yielded lipid membranes retaining macrophage's biomarkers (Fig. 1B). Subsequent fusion with pre-formed Emo-loaded liposomes (Emo-LPs) was confirmed through multiple analytical techniques. Transmission electron microscope (TEM) revealed the characteristic core-shell nanostructure with an apparent outer membrane layer (Fig. 1C). Dynamic light scattering (DLS) demonstrated a significant reduction in size from 152.9 nm (Emo-LPs) to 131.2 nm (Emo-*mc*NVs) (Fig. 1D) with low polydispersity index (PDI) (0.238) and high entrapment efficiency (EE 99.4 %). Zeta potential measurements showed a clear shift from −2.46 mV (Emo-LPs) to −18.3 mV (Emo-*mc*NVs), closely matching native macrophage membrane charge [21]. In addition, the macroscopic transition from a translucent to a slightly opalescent solution provided further qualitative validation (Fig. 1E). These results collectively confirm the successful integration of macrophage membranes into the nanovesicles while preserving drug loading integrity. Detailed experimental methods for the preparation, characterization, and subsequent analysis of Emo-*mc*NVs are provided in Supporting information.

The *in vitro* release behaviors of Emo-LPs and Emo-*mc*NVs were comparatively evaluated under simulated physiological conditions (deionized water, 0.1 mol/L HCl, and pH 7.2 phosphate buffer saline (PBS)). Notably, Emo-*mc*NVs exhibited consistently slower and lower drug release kinetics than Emo-LPs across all tested conditions (Fig. 1F), which is advantageous for disease treatment as it allows the nanocarriers to maintain their structural integrity and exert therapeutic effects in their intact modality [22]. In acidic environment (0.1 mol/L HCl), Emo-*mc*NVs demonstrated a retarded drug release profile after 4 h, indicating the macrophage membrane coating impeded premature payload leakage. The differential release became particularly pronounced at colonic pH (7.2 PBS), where Emo-*mc*NVs maintained substantially lower accumulative release compared to the counterparts throughout the observation period (paired *t*-test, $P < 0.01$). While both formulations displayed similar initial burst release characteristics in deionized water, Emo-*mc*NVs again showed more sustained release kinetics beyond the 4-h timepoint. This disparate release behavior can be attributed to three key advantages conferred by the biomimetic membrane cloaking: (1) Enhanced membrane retardancy from drug release, (2) improved site-specific delivery matching the temporal requirements of ulcerative colitis therapy, and (3) increased resistance to lipolysis in the gastrointestinal tract [23]. These results demonstrate that the biomimetic membrane coating effectively modulates Emo release kinetics while providing physiological protection [24].

The cell uptake analysis revealed that Emo-*mc*NVs exhibited faster and stronger internalization compared to Emo-LPs, as evidenced by the more intense DiO fluorescence signal colocalized with Hoechst-stained nuclei in the merged images (Fig. 2A). Quan-

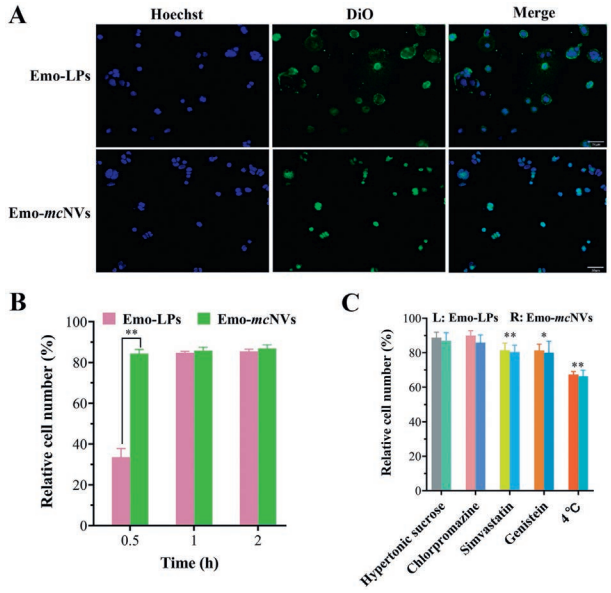


Fig. 2. Cellular uptake and internalization of Emo-LPs and Emo-*mc*NVs. (A) Confocal laser scanning microscopy (CLSM) images of cellular internalization upon co-incubation for 0.5 h. Scale bar: 50 μm. (B) Cellular uptake quantified by flow cytometry ($^{**}P < 0.01$, paired *t*-test). (C) Relative cellular uptake in the presence of transport inhibitors or under 4 °C (L: left, R: right. ANOVA with Tukey's test, $^{*}P < 0.05$, $^{**}P < 0.01$ vs. control). Data expressed as mean ± SD ($n = 3$).

titative data demonstrated time-dependent uptake, with Emo-*mc*NVs showing significantly higher cellular association at an early time point (Fig. 2B), suggesting enhanced interaction with cells due to the macrophage membrane coating. Both Emo-*mc*NVs and Emo-LPs likely shared similar endocytic pathways such as energy-dependent membrane mobile transport (cytosis) and caveolin-mediated endocytosis (Fig. 2C) [25], but the natural ligands on the macrophage membrane of Emo-*mc*NVs further promoted receptor-mediated internalization [26]. This improved uptake efficiency, combined with the previously observed sustained drug release profile, supports the potential of Emo-*mc*NVs for targeted intracellular drug delivery applications. The biological membrane cloaking not only facilitated cellular entry but also contributed to prolonged intracellular retention, thus aligning with the therapeutic goal of achieving effective drug accumulation at disease sites.

The therapeutic efficacy of Emo-*mc*NVs was comprehensively evaluated in DSS-induced colitis mice. All animal experiments were conducted in strict accordance with The Guide for the Care and Use of Laboratory Animals (NRC) and were approved by Jinan University's Animal Ethics Committee. Emo-*mc*NVs demonstrated remarkable therapeutic effects in the murine UC model through a multifaceted mechanism of action. As shown in Fig. 3, treatment with Emo-*mc*NVs effectively alleviated key pathological manifestations of ulcerative colitis. The induction and treatment protocol for UC is illustrated in Fig. 3A. Treatment with Emo-*mc*NVs significantly mitigated body weight loss and reduced disease activity index (DAI) scores during the early intervention phase (Figs. 3B and C), indicating substantial improvement in curative outcomes. The preservation of colon length and decreased serum levels of pro-inflammatory cytokines (tumor necrosis factor α (TNF-α), interleukin 1β (IL-1β), and IL-6) suggested systemic anti-inflammatory activity (Figs. 3D–H). Histopathological examinations revealed that Emo-*mc*NVs effectively preserved mucosal architecture while substantially diminishing both inflammatory infiltration and fibrotic deposition in the colonic tissue (Figs. 3I and J). This multimodal therapeutic approach results in enhanced tissue protection and re-

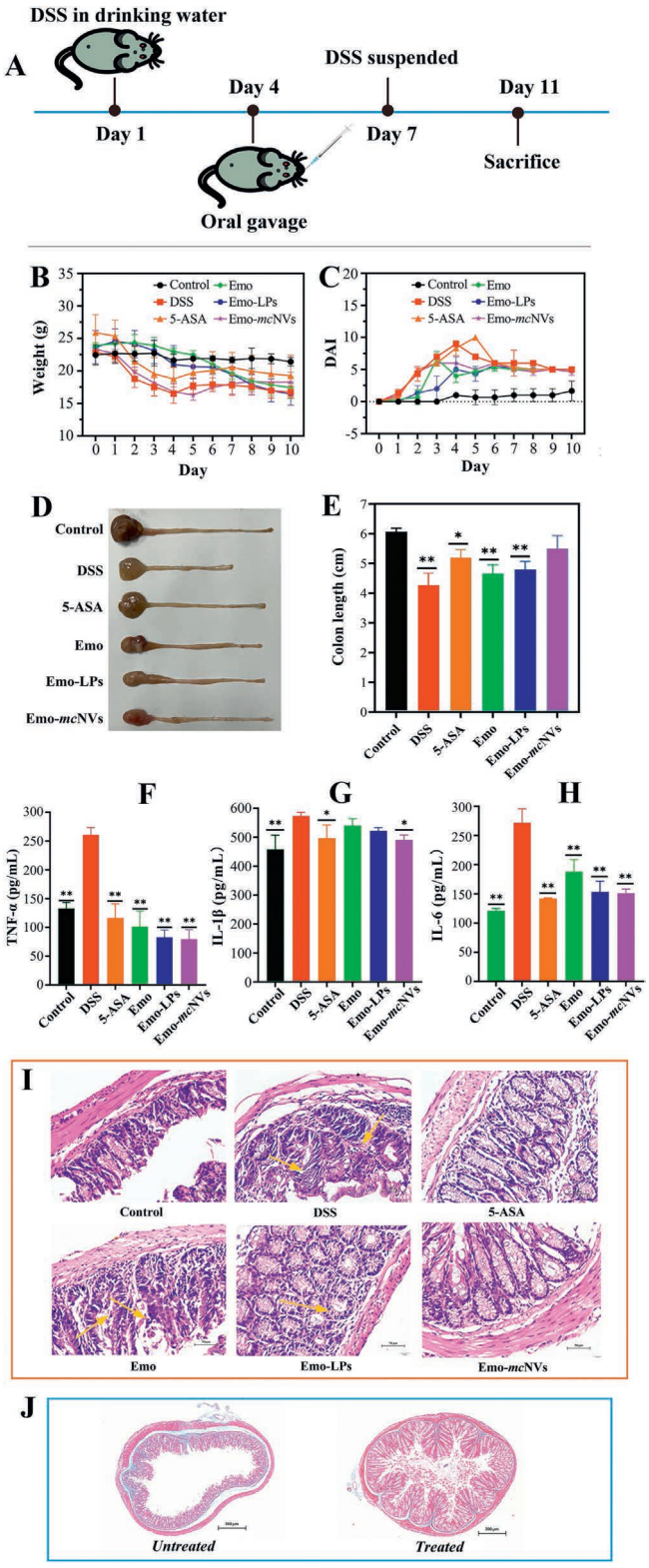


Fig. 3. Anti-colitis effects of Emo-*mc*NVs in a DSS-induced UC model. (A) Schematic of experimental design: DSS administration in drinking water (days 1–7) and treatment by oral gavage (days 4–11). (B) Body weight changes. (C) DAI score. (D, E) Representative colon images and colon length quantification ($^{**}P < 0.01$ *vs.* control, ANOVA). (F–H) Serum levels of TNF-α, IL-1β, and IL-6 ($^{*}P < 0.05$, $^{**}P < 0.01$ *vs.* DSS group). Data expressed as mean ± SD ($n = 3$). (I) Colon histopathology by hematoxylin-eosin (H.E.) staining (yellow arrows indicate inflammatory infiltration). Scale bar: 50 μm. (J) Fibrosis assessment by Masson's trichrome staining after treatment (blue: collagen deposition). Scale bar: 200 μm.

generation compared to conventional treatments and other Emo formulations.

The superior efficacy of Emo-*mc*NVs compared to free Emo or 5-aminosalicylic acid (5-ASA, a positive control drug) may be attributed to their targeted delivery and sustained release properties, which enhance drug accumulation in the inflamed colon tissues while minimizing systemic side effects [27,28]. Although previous studies have demonstrated Emo's anti-UC potential through its anti-inflammatory (proinflammatory cytokine and signaling pathway suppression), antioxidant, and epithelial barrier-protective effects [29–32], its clinical application remains limited by poor solubility and non-specific biodistribution. Our engineered Emo-*mc*NVs effectively overcome these limitations. Emo-*mc*NVs primarily achieve colonic accumulation and therapeutic improvement through chemotactic homing to inflamed tissues [33,34], mediated by their interactions with inflammatory cells and vascular endothelium in UC lesions. This targeted delivery approach enables synergistic modulation of multiple pathological processes in UC, including inflammation, oxidative stress and fibrosis [35,36], resulting in profitable attenuation in DAI compared to 5-ASA. The performance of Emo-*mc*NVs surpasses both conventional therapies and previously reported Emo formulations [37], such as hydrogels and lipid nanoparticles.

To elucidate the underlying mechanisms responsible for the enhanced therapeutic effects of Emo-*mc*NVs, we systematically evaluated their biodistribution using multimodal imaging approaches with an FD-B21 fluorescent probe [38]. Two-dimensional real-time tracking was conducted using the IVIS Lumina Series III imaging system (PerkinElmer), while three-dimensional spatial mapping was performed with the InSyTe FLECT/CT platform (TriFoil), which integrates fluorescence molecular tomography with anatomical X-ray CT for enhanced spatial resolution. Two-dimensional small animal *in vivo* imaging revealed a distinct pattern of fluorescence accumulation in the Emo-*mc*NVs group, with pronounced colonic localization observed particularly after 8 h post-administration. In contrast, Emo-LPs exhibited a more dispersed fluorescence signal across multiple tissues, indicating a non-specific distribution pattern (Fig. 4A). This finding strongly supports the superior colon-targeting properties of Emo-*mc*NVs. *Ex vivo* imaging further corroborated these results, demonstrating significant colonic accumulation of Emo-*mc*NVs (as indicated by arrows), while Emo-LPs showed widespread distribution throughout the intestinal tract (Fig. 4B). Notably, both Emo-LPs and Emo-*mc*NVs displayed minimal accumulation in vital organs (heart, liver, spleen, lungs, and kidneys), with predominant localization in the gastrointestinal tract, thereby effectively mitigating potential systemic toxicity risks. At the 8-h time point post-administration, we performed combined computerized tomography (CT) and fluorescence imaging on depilated mice. Three-dimensional reconstruction analysis confirmed the differential distribution patterns, revealing multi-tissue dispersion of Emo-NVs alongside concentrated colonic localization of Emo-*mc*NVs (Fig. 4C), in agreement with two-dimensional *in vivo* imaging results. FD-B21 is a novel absolute aggregation-caused quenching (aACQ) probe that exhibits fluorescence in its uniformly dispersed state but undergoes quenching upon aggregation [39]. This unique property enables precise prediction of nanocarriers' *in vivo* fate. Notably, the fluorescence signal specifically reflects intact nanocarriers rather than released fluorescent molecules, since the latter tend to aggregate and consequently lose fluorescence. Owing to these advantages, aACQ technology has emerged as a powerful tool for tracking the *in vivo* behavior of nanocarriers [40–43]. The concordance between two- and three-dimensional (2D and 3D) *in vivo* imaging, complemented by *ex vivo* imaging data, provides robust evidence for the colon-specific targeting capability of Emo-*mc*NVs. This targeted delivery mechanism fundamentally explains the enhanced therapeutic performance of

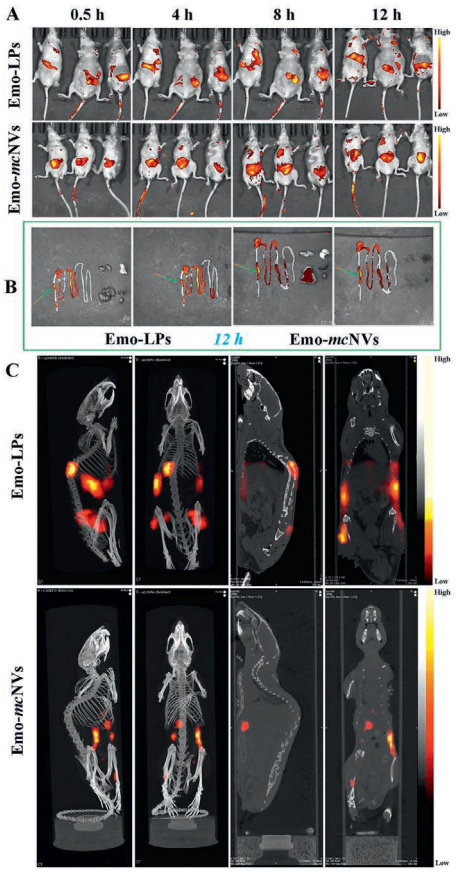


Fig. 4. *In vivo* temporal distribution profiles of Emo-LPs and Emo-*mc*NVs in murine UC model. (A) Time-dependent accumulation patterns post-administration captured by 2D *in vivo* imaging. (B) *Ex vivo* imaging of intestinal biodistribution, a comparison between Emo-LPs and Emo-*mc*NVs (arrows highlight colon-specific localization). (C) 3D reconstructed mapping of colonic distribution at 8 h post-administration, aligned with therapeutic activity timelines in former assays.

Emo-*mc*NVs in UC treatment, as it ensures precise drug delivery to the affected colonic tissues while minimizing off-target effects and systemic exposure [44–46]. The temporal distribution patterns observed at 0.5, 4, 8, and 12 h (as indicated in the reference images) further support the sustained colon retention of Emo-*mc*NVs, which likely contributes to their prolonged therapeutic action at the disease site.

Chemokines are small signaling proteins that recruit immune cells to inflammatory sites, playing pivotal roles in immune responses, inflammation, and cell migration [47]. They are implicated in various diseases, such as rheumatoid arthritis, atherosclerosis, and neuropathy [48]. Upon stimulation by tissue cells, immune cells or pathogens, chemokines are secreted. These chemokines form concentration gradients at inflammatory sites either by binding to extracellular matrix components or *via* free diffusion, with higher concentrations directing immune cells toward the inflammatory core. Macrophages, which express multiple chemokine receptors [49], migrate along these gradients *via* receptor-ligand interactions.

To elucidate the role of chemokine-mediated macrophage recruitment in UC, we measured the expression of CCL2, CCL3, and CCL5, three key macrophage-associated chemokines, in colon tissues of healthy and UC-modeled mice using enzyme-linked immunosorbent assay (ELISA). As shown in Table 1, all three chemokines exhibited significantly elevated expression in UC colons compared to normal tissues ($P < 0.01$), consistent with prior findings [50]. This chemokine upregulation establishes a strong

Table 1
Chemokine expression in the normal colon and ulcerative colon.

Chemokine	Normal colon	Ulcerative colon
CCL2	87.51 ± 3.62	$653.27 \pm 6.84^{**}$
CCL3	35.84 ± 4.45	$175.47 \pm 5.17^{**}$
CCL5	37.66 ± 2.78	$156.29 \pm 4.26^{**}$

Note: Measurements were performed through mouse ELISA kits. Data expressed as mean ± SD ($n = 3$), $^{**}P < 0.01$, paired *t*-test, compared with normal group; concentration: pg/100 mg colonic tissue.

chemoattractant gradient that directs the targeted migration of Emo-*mc*NVs to inflamed colon tissues, mirroring the chemotaxis-driven delivery strategy employed in tumor-targeting nanotherapeutics [51].

Our engineered Emo-*mc*NVs exploit this endogenous targeting mechanism through active chemotactic navigation, similar to NETs-targeting systems [52], achieving site-specific drug delivery by leveraging pathological chemokine gradients. This pathophysiology-guided approach represents a novel therapeutic strategy for UC that aligns with current trends in nanomedicine. The macrophage membrane biomimicking confers distinct advantages over conventional synthetic nanocarriers, including enhanced chemokine receptor-mediated targeting comparable to macrophage-derived exosome systems [53], as well as improved biocompatibility and prolonged circulation time characteristic of biomimetic platforms [54]. Although scale-up production presents challenges, these may be overcome through innovative hybrid engineering approaches [55].

In conclusion, this study demonstrates the successful development of macrophage membrane-engineered nanovesicles as an innovative delivery system for targeted UC treatment. By leveraging the innate chemotactic properties of macrophage membranes combined with synthetic liposomal carriers, the engineered Emo-*mc*NVs achieved successful colonic targeting through chemokine gradient recognition while maintaining excellent drug loading capacity and stability. The bioinspired nanovesicles demonstrated superior therapeutic effects in a murine UC model, including reduced disease activity, preserved colon morphology and attenuated inflammatory responses, outperforming both free Emo and standard 5-ASA treatment. This work establishes a novel biomimetic strategy that exploits disease pathophysiology for targeted drug delivery, offering significant potential for improving inflammatory bowel disease therapy. The findings not only advance UC treatment options but also provide a platform technology adaptable to other chemokine-driven inflammatory diseases. Future studies should focus on clinical translation and expanding applications of this promising nanomedicine approach.

Declaration of competing interest

The authors declare that they have no known competing financial interests or personal relationships that could have appeared to influence the work reported in this paper.

CRediT authorship contribution statement

Youcheng Hu: Writing – original draft, Methodology, Investigation, Formal analysis. **Guichan Li:** Validation, Methodology, Investigation, Data curation. **Chunli Qi:** Validation, Investigation. **Xiaoyan Lin:** Methodology, Investigation. **Xingwang Zhang:** Writing – review & editing, Supervision, Project administration, Funding acquisition, Conceptualization. **Hao Wang:** Writing – review & editing, Supervision, Project administration, Funding acquisition, Conceptualization.

Acknowledgments

This work was jointly supported by Science and Technology Project of Guangzhou (No. 2023B03J1353), Clinical Characteristic Technology Project of Guangzhou Municipal Health Commission (No. 2023P-TS28), "Guangdong Special Support Plan" – Provincial Health Commission (Health Talent) Project (No. 0720240108), and Guangdong Basic and Applied Basic Research Foundation (Nos. 2025A1515011285, 2023A1515012326).

Supplementary materials

Supplementary material associated with this article can be found, in the online version, at doi:10.1016/j.cclet.2025.111727.

References

[1] V. Jairath, N. Narula, R.C. Ungaro, et al., J. Crohns Colitis 19 (2025) jjaf040.
[2] A. Di Rienzo, L. Marinelli, M.P. Dimmito, et al., Pharmaceutics 16 (2024) 1185.
[3] P. Wangchuk, K. Yeshi, A. Loukas, Trends Pharmacol. Sci. 45 (2024) 892–903.
[4] Y. Liang, Y. Li, C. Lee, et al., Mol. Biomed. 5 (2024) 42.
[5] J. Zhao, S. Hao, Y. Chen, et al., Colloids Surf. B: Biointerfaces 236 (2024) 113798.
[6] S. Luo, J. He, S. Huang, et al., Phytomedicine 104 (2022) 154106.
[7] Y.Y. Xu, M. Zhu, J. Wu, et al., Chin. Med. 18 (2023) 98.
[8] Z. Ai, B. Liu, J. Chen, et al., Int. J. Pharm. X 9 (2025) 100314.
[9] X. Chen, X. Ling, L. Zhao, et al., ACS Appl. Mater. Interfaces 10 (2018) 33976–33985.
[10] F. Xiong, X. Ling, X. Chen, et al., Nano Lett. 19 (2019) 3256–3266.
[11] Z. Fang, X. Zhang, H. Huang, et al., Chin. Chem. Lett. 33 (2022) 1693–1704.
[12] Y. Wang, C. Zhang, S. Han, et al., Chin. Chem. Lett. 35 (2024) 109578.
[13] H.L. Wang, Z. Peng, Y.Q. Li, et al., Inflamm. Res. 73 (2024) 1267–1282.
[14] A.J. Burnham, A.I. Toma, D. Shah, et al., Cytotherapy 27 (2025) 338–349.
[15] Y. Qian, Z. Yan, T. Ye, et al., Exploration 4 (2024) 20230098.
[16] C. Gu, X. Geng, Y. Wu, et al., Small 20 (2024) e2305659.
[17] A. Zhou, K. Chen, Y. Gao, et al., ACS Nano 17 (2023) 16461–16477.
[18] M.J. Zhu, S.P. Zhu, Q.B. Liu, et al., Chin. Chem. Lett. 34 (2023) 107482.
[19] Y.T. Sato, K. Umezaki, S. Sawada, et al., Sci. Rep. 6 (2016) 21933.
[20] C.L. Lin, Z.S. Fang, C.Y. Hsu, et al., Acta Biomater. 173 (2024) 325–335.
[21] D. Hu, Z. Huang, W. Li, et al., Mol. Pharm. 22 (2025) 771–786.
[22] Y. Ma, H. He, W. Fan, et al., ACS Biomater. Sci. Eng. 3 (2017) 2399–2409.
[23] O.J. Hedge, F. Höök, P. Joyce, et al., Langmuir 37 (2021) 10200–10213.
[24] N. Jan, A. Madni, S. Khan, et al., Bioeng. Transl. Med. 8 (2023) e10441.
[25] Y. Li, C. Zhu, Int. J. Nanomedicine 12 (2017) 1673–1684.
[26] L. Hou, X. Gong, J. Yang, et al., Adv. Mater. 34 (2022) e2200389.
[27] K. Dong, S.J. Deng, B.Y. He, et al., Drug Des. Devel. Ther. 17 (2023) 191–207.
[28] J. Xian, X. Zhong, H. Gu, et al., Pharmaceutics 13 (2021) 2025.
[29] S. Luo, X. Deng, Q. Liu, et al., Int. Immunopharmacol. 59 (2018) 269–275.
[30] Y. Zhang, W. Pu, M. Bousquenaud, et al., Front. Oncol. 10 (2020) 564674.
[31] D. Yang, T. Ge, J. Zhou, et al., Heliyon 10 (2024) e34932.
[32] Y. Li, R. Guo, M. Zhang, et al., Exp. Ther. Med. 19 (2020) 3521–3530.
[33] H.I. Tong, W. Kang, P.M. Davy, et al., PLoS One 11 (2016) e0154022.
[34] W. Yu, B. Li, L. Chen, et al., J. Ethnopharmacol. 328 (2024) 118123.
[35] L. Xu, J. Gao, D. Huang, et al., Biochem. Biophys. Res. Commun. 534 (2021) 279–285.
[36] D. Yan, Y. Wei, X. Ye, et al., ACS Appl. Mater. Interfaces 17 (2025) 13676–13689.
[37] H. Luo, X. Ji, M. Zhang, et al., Mini Rev. Med. Chem. 24 (2024) 1784–1798.
[38] Y. Cai, X. Ji, Y. Zhang, et al., Aggregate 4 (2023) e277.
[39] H. He, C. Liu, J. Ming, et al., Aggregate 3 (2022) e163.
[40] W. Fan, H. Peng, Z. Yu, et al., Acta Pharm. Sin. B 12 (2022) 2479–2493.
[41] C. Liu, Y. Cai, Z. Zhang, et al., Acta Pharm. Sin. B 14 (2024) 3155–3168.
[42] Z. Zhang, C. Liu, Y. Lu, et al., J. Nanobiotechnology 22 (2024) 488.
[43] X. Ji, A. Raza, J. Qi, et al., J. Pharm. Anal. 15 (2025) 101044.
[44] X. Wu, Q. Zhang, L. Peng, et al., J. Mater. Chem. B 12 (2024) 1604–1616.
[45] S. Fan, Y. Zhao, Y. Yao, et al., J. Transl. Med. 22 (2024) 878.
[46] Z. Zhuo, K. Guo, Y. Luo, et al., Theranostics 14 (2024) 528–546.
[47] C.E. Hughes, R.J.B. Nibbs, FEBS J. 285 (2018) 2944–2971.
[48] K. Wang, Y. Wang, L. Wang, et al., Chin. Chem. Lett. 36 (2025) 109868.
[49] Y. Song, Y. Huang, F. Zhou, et al., Chin. Chem. Lett. 33 (2022) 597–612.
[50] S. Melgar, M. Drmotova, E. Rehnström, et al., Cytokine 35 (2006) 275–283.
[51] M. Li, S. Li, H. Zhou, et al., Nat. Commun. 11 (2020) 1126.
[52] T. Zhang, P. Liu, W. Shen, et al., Adv. Sci. 12 (2025) e03689.
[53] Y. Li, Z. Cai, Z. Wang, et al., Chin. Chem. Lett. 36 (2025) 109942.
[54] Y. Yu, T. Li, M. Ou, et al., J. Control. Release 365 (2024) 469–479.
[55] Y. Yu, F. Zhang, W. Xiao, et al., ACS Nano 18 (2024) 5915–5929.